

Processing and characterization of biodegradable polymer nanocomposites: detection of dispersion state

Natalia V. Pogodina · Claire Cerclé · Luc Avérous ·
Ralph Thomann · Michel Bouquey · René Muller

Received: 28 June 2007 / Accepted: 6 November 2007 / Published online: 13 January 2008
© Springer-Verlag 2007

Abstract Nanobiocomposites of poly(lactic acid) (PLA) with 3–5 wt% organically modified montmorillonite (OMMT) were prepared by melt compounding in two different mixers, miniature twin-screw extruder and internal batch mixer, leading to different degrees of dispersion. The progress of dispersion was characterized by melt rheology coupled with light attenuation. Processed PLA/OMMT samples showed percolating networks in the melt, detected by a step increase in low-frequency elastic moduli. The melt elasticity of nanocomposites increased, while the light attenuation coefficient and the loss tangent decreased progressively with mixing energy and reached saturation that can be attributed to the maximum level of clay

dispersion achieved in the present experimental conditions. Results showed that a combination of low-frequency loss tangent and light attenuation coefficient provides a potentially sensitive method for the characterization of the degree of clay dispersion. The direct correlation between light attenuation coefficient and loss tangent follows linear dependence and may open an approach for the rapid inline analysis of the degree of dispersion in melt-processed nanocomposites.

Keywords Nanobiocomposites · Degree of dispersion · Percolating network · Light attenuation · Melt elasticity

Paper presented at the 4th Annual European Rheology Conference (AERC), April 12–14, 2007, Naples, Italy.

N. V. Pogodina · C. Cerclé · L. Avérous · M. Bouquey · R. Muller (✉)
Laboratory of High Technology Polymeric Materials,
ECPM-LIPHT (UMR CNRS 7165),
Louis Pasteur University,
25 rue Becquerel,
67087 Strasbourg, Cedex 2, France
e-mail: Rene.Muller@ecpm.u-strasbg.fr

N. V. Pogodina
e-mail: Natalia.pogodina@ecpm.u-strasbg.fr

C. Cerclé
e-mail: cerclec@hotmail.fr

L. Avérous
e-mail: averousl@ecpm.u-strasbg.fr

M. Bouquey
e-mail: bouqueym@ecpm.u-strasbg.fr

R. Thomann
Freiburger Materialforschungszentrum,
Stefan-Meier-Str. 21,
79104 Freiburg i. Br., Germany
e-mail: ralf.thomann@fmf.uni-freiburg.de

Introduction

Polymer–clay nanocomposites (PNC) are multiphase systems based on components with vastly different properties in the nanometer scale. These materials exhibit many unique properties, such as improved thermal stability, reduced flammability, and improved mechanical and barrier properties, which makes them commercially valuable. The uniform and high level of dispersion of nanoscopically sized fillers (exfoliation process) is the key to the valuable properties of PNC. This uniform dispersion of nanofillers on the order of a few nanometers produces large interfacial area. When polymer–nanoparticle interphase is tailored by a certain compatibility level between the phases, nanocomposites show optimized performance.

Several approaches are developed to exfoliate the initially microscopically heterogeneous system to a nanoscopically homogeneous, including solution processing, in situ polymerization, and melt processing technique. The latter one is very attractive for industrial application due to its simplicity. Despite extensive research and vast amount of publications in the field of polymer nanocomposites (Pinnovaia and Beall

2001; Utracki 2004), the industrial fabrication of PNC is still based on a semiempirical approach. The lack of fundamental understanding of interphase–morphology–property relationships in PNC materials limits our possibility to control their processing and performance. The situation is even more complex when PNC are based on environmentally friendly biodegradable polymers. Among those, poly(lactic acid) (PLA) is at present one of the most promising, commercially available biodegradable polymer with a large range of grades (Ray and Okamoto 2003).

The dispersion morphology and the interphase that impart the valuable properties to the PNC material are born at the processing step. Which processing factor imparts the better level of dispersion is still under discussion. High stresses developed in high viscous matrix (Fornes et al. 2001) and long residence times (Dennis et al. 2001) were pointed out as the key parameters for dispersing clay stacks. Recently, it has been shown that better dispersion was achieved in low viscous matrices (Tanoue et al. 2004). Simultaneous rheo-X-ray studies showed (Bousmina 2006) that the best level of the dispersion requires a balance between the diffusion of polymer chains in interlayer spacing and mechanical shearing to break up clay stacks. According to the author, the medium matrix viscosity and two-step processing (low shear followed by high shear) gives optimum results.

Another important question is how to control the degree of clay dispersion. The morphology of the processed nanocomposite is very complex and may include micro-particles, tactoids, and individual layers (Szazdi et al. 2006). Existing experimental methods probe the complex structure of nanocomposites on different length scales. Transmission electron microscopy (TEM) and X-ray scattering provide local structural characterization on a small scale (Fornes et al. 2001; Dennis et al. 2001; Szazdi et al. 2006; Bousmina 2006). Rheological and mechanical tests probe the bulk of the nanocomposite material and sense the changes in the dispersion process of clay agglomerates on a large scale (Wagener and Reisinger 2003; Meincke et al. 2004; Kadar et al. 2006).

The aim of this paper is to study the influence of processing (the type of compounding device, shear rate, mixing time, mixing energy) on the degree of dispersion of clay stacks in a biodegradable polymer matrix with respect to the rheological, structural, and optical properties and to develop an approach for the rapid analysis of the progress of dispersion.

Experimental part

Materials

The PLA used in this work was supplied by Nature Work[®] (Cargill-Dow LLC, USA). As it was reported by Martin and

Avérous (2001), this biodegradable polyester consists of 92% L-lactide and 8% mesolactide contents. The weight-average molecular weight $M_w=108,000$ g/mol and the polydispersity index $M_w/M_n=1.7$ were determined by size exclusion chromatography (SEC). The glass transition and melting temperatures as determined by differential scanning calorimetry (DSC) are 60 and 155 °C, respectively. Density is 1.25 g/cm³ at 25 °C. The organically modified montmorillonite (OMMT) used in this study was supplied by Southern Clay Products (Cloisite[®] 30B). Cloisite 30B is organically modified by methyl bis-2-hydroxyethyl hydrogenated tallow ammonium. The content in organics is 30 wt% for Cloisite 30B.

Compounding and specimen preparation

PLA (pellets form) and clay (powder form) were dried overnight at 80 °C under vacuum. Before processing, 3 and 5 wt% of OMMT have been added into the PLA and premixed in a plastic bag. The compounding of PLA/OMMT nanobiocomposites was carried out at 170 °C in the two mixers: Minilab microcompounder (Rheomex CTW5, Thermolectron) and an internal batch mixer (Rheocord 9000, Haake) at different processing conditions, varying screw speed, and mixing time. The Minilab is a miniature twin-screw extruder with a small filling polymer mass of 5–6 g and an automatic bypass for recirculation. The microcompounder can be equipped with conical corotating or counterrotating screws. The Rheocord 9000, Haake internal batch mixer operates with two blades in counterrotating configuration and a much bigger polymer mass, about 50 g.

Rheological characterization

The samples processed in both mixers were compression molded into 25 mm diameter disks, 1 mm thick, at 170 °C between two metal blocks lined with Teflon-coated foil using a heated laminating press.

These disks were used for rheological experiments. Dynamic rheological measurements were performed using an advanced rheometric expansion system (ARES) from Rheometrics (TA Instruments). The measurements were carried out in an oscillatory mode using parallel plates (25 mm diameter) at 170 °C. Frequency sweeps were carried out in the range 0.01–100 rad/s at the strain amplitude of 10% to stay in linear viscoelastic range.

Light attenuation

Turbidity was measured at room temperature on solid samples, compression molded as discussed above into disks, 1 mm thick and 25 mm diameter. Linearly polarized light from a 1-MW He–Ne laser (wavelength 632.8 nm)

passes through the sample and is focused by an objective on a silicone photodiode (Thorlabs, DET 36A/M) for intensity recording, using a data acquisition board (National Instruments, NI-USB-6009). The transmitted intensity from pure laser and from all the samples was monitored with a sampling rate of 0.2 s for 5 min at three different positions for each sample. The results were averaged to minimize the error from possible intensity fluctuations caused by the laser. The averaged intensities have been used to estimate the attenuation coefficient.

X-ray diffraction

The small angle X-ray scattering (SAXS) measurements were carried out on a powder diffractometer Siemens D 5000 (Germany) using Cu ($K\alpha$) radiation, $\lambda=0.15406$ nm, in the range of $2\theta=1.0^\circ$ to 10° by step of 0.05° per 1 s. SAXS analysis was performed at room temperature for pure Cloisite 30B and nanocomposite samples, processed in the batch mixer and in the microextruder. For these tests, the specimens were prepared by compression molding at $T=170^\circ\text{C}$, as already described above.

Mechanical characterization

After melt processing, the molten materials were injection molded (170°C , 250 MPa) in the shape of standard dumbbell specimens (tensile bar ASTM D638), using the minijet injection molding machine (Thermo Electron Corporation, Germany).

Tensile tests were performed for PLA and all samples with a MTS 2/M instrument (Adamel Lhomargy, Ivry sur Seine, France) at room temperature with a speed of 5 mm/min.

Results and discussion

Mixing

Compounding of the nanocomposites was performed with intensive mixing in the internal batch mixer and in the miniature twin-screw extruder with corotating configuration of screws where the clay stacks and polymer matrix are subjected to shearing in the flow field.

Both rotational mixers have been approximated by the Couette geometry. The shear rate is then given by (Maric and Macosko 2001):

$$\dot{\gamma} = \frac{D\Omega}{2h} \quad (1)$$

where D is the average screw diameter, h is the average gap between the screws and the barrel, $\Omega=2\pi N/60$ is the angular velocity in rad/s, and N is the screw speed in

revolution per minute. Index 1 is used for the Minilab and index 2 is used for the internal batch mixer. Equation 1 gives only a rough approximation of the “average” shear rate. As it has been shown by Bousmina et al. (1999), local shear rates can be orders of magnitudes different at various locations, especially if two different mixers with different screw configurations and different flow fields are compared.

The Minilab has conical screws, so the average D_1 and h_1 values have been taken in the middle of the screw $D_1=10$ mm, $h_1=0.5$ mm. For the Haake batch mixer: $D_2=36$ mm, $h_2=2$ mm. The screw speeds for the batch mixer were $N_2=50$ and 100 rpm. For the Minilab, a broader range of mixing speeds (and shear rates) was explored: $N_1=12$, 25, 50, 100, and 200 rpm. The maximum average shear rate achieved in the batch mixer was 600°s^{-1} , while in the Minilab it was twice as large $1,314^\circ\text{s}^{-1}$. The mixing times in the batch mixer were correspondingly $t_2=5$, 10, and 20 min, while in the miniextruder, the longer times have been used: $t_1=7$, 15, 30, and 50 min. Thus, higher shear rates and higher total strains have been applied in the Minilab.

Because we used two different mixers with different capacities and varied processing conditions, it was reasonable to compare the resultant characteristics of the processed nanocomposites as a function of mixing energy E . For the rotational mixer, the mixing energy per unit mass can be expressed as:

$$E = \frac{T\Omega t}{M} \quad (2)$$

where T is the torque, t is the mixing time, and M is the loaded mass. Due to longer mixing times and higher mixing speed, the maximum mixing energy achieved in the Minilab was about four times higher than in the batch mixer.

Melt rheology

Rheology probes the material properties in the bulk. So it has the advantage of being able to detect the three-dimensional superstructures. Especially fruitful are rheological experiments in the small amplitude oscillatory shear (SAOS) mode. First, SAOS uses small strain amplitudes and consequently does not disrupt the possible network formation. These conditions are especially important for nanocomposites which incorporate stiff anisometric clay particles in the matrix. Second, dynamic moduli in the low-frequency range respond very sensitively to the melt elasticity and to the formation of three-dimensional structures. Network formation has been reported in various nanocomposite systems (Wagener and Reisinger 2003; Meincke et al. 2004; Kadar et al. 2006).

A rheological method for the detection of network-like structure formation was proposed by Winter and Mours

(1997). Although originally the method was developed for the detection of chemical gelation (upon the increasing degree of crosslinking), it was successfully used later for the detection of physical gels during crystallization in semicrystalline polymers and gel-like structures in long-chain branched polymer melts.

According to the authors, at the critical gel point, the low-frequency dynamic moduli show a power law behavior:

$$G_c' = \frac{G_c''}{\tan \delta_c} = S_c \Gamma(1 - n_c) \cos \frac{n_c \pi}{2} \omega^{n_c} \quad \text{for } \omega < 1/\lambda_0 \quad (3)$$

where S_c and n_c are the gel stiffness and the relaxation exponent, respectively, and λ_0 is the lower crossover. All three parameters depend on the material structure at the transition. Γ is the gamma function. A consequence of this power law behavior (at the gel point) is a frequency-independent loss tangent in the terminal zone.

$$\tan \delta_c = \tan \frac{n_c \pi}{2} = \frac{G''}{G'} = \text{const} \quad (4)$$

The formation of a network-like structure (the instant of the liquid-to-solid transition, i.e., critical gel point) is identified by $\tan \delta(\omega)$ becoming independent of the frequency in the terminal zone according to Eq. 4. After the gel point, i.e., after the liquid–solid transition, the network also exists and the material shows solid-like behavior, which is identified by the positive slope of $\tan \delta(\omega)$ in the terminal zone.

Figure 1a and b shows the evolution of the storage modulus and $\tan \delta$ as a function of frequency ω for the pure PLA and PLA–clay systems processed in two different mixers with varying shear rates and mixing time. Within the accessible frequency range, G' for pure PLA is close to the typical low-frequency asymptote of slope 2 for a viscoelastic liquid. The PLA–clay samples reveal in the terminal zone progressively higher elasticity (higher values of the dynamic moduli G' , G'' , and lower phase angle). Melt elasticity increases with the increase of the screw speed (shear rate), mixing time, and clay concentration. The fact that, for a given mixing device, the mixing time is suited for better dispersion indicates the eventual role of diffusion in the dispersing process. Moreover, there is a great difference in the rheological response of PLA–clay systems processed in the two different mixers: the low-frequency storage modulus of nanocomposites processed in the Haake batch mixer is one order of magnitude higher and nearly frequency-independent, while the elastic response of nanocomposites processed in the Minilab microextruder is much weaker for the same concentration 3 wt% (Fig. 1a). We argue that this drastically different level of melt elasticity is due to the different degree of clay dispersion in processed nanocomposites, which results in morphologically different network structures.

Figure 1b shows that in the low-frequency range, the slope of $\tan \delta(\omega)$ changes from negative for pure PLA (typical for the liquid-like behavior) to positive for PLA–clay (typical for the solid-like behavior). It means that the solid-like network of percolating nanoclay fillers in the PLA matrix is monitored for PLA nanocomposites processed in both mixers.

Another representation of the network formation phenomena is given by the van Gurp plot. In the van Gurp plot, the phase angle $\delta = \arctan G''/G'$ is plotted vs the complex

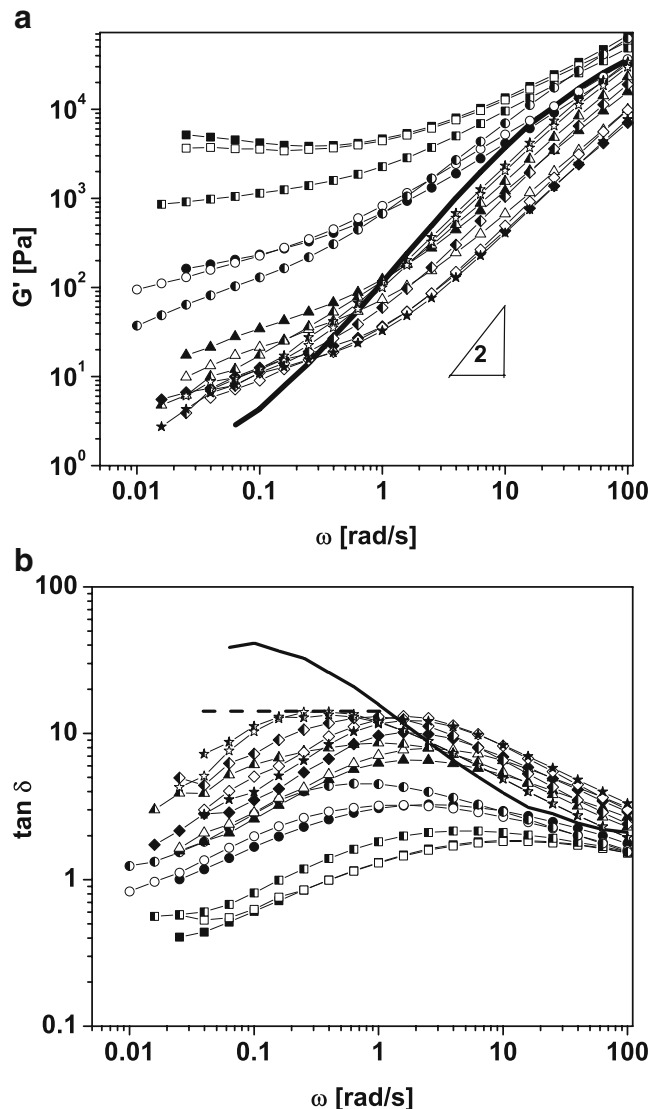


Fig. 1 Evolution of **a** storage modulus and **b** loss tangent for the PLA, PLA/OMMT-3 wt%, and PLA/OMMT-5 wt% compounded at different processing conditions and in two mixers. The gel point in **b** is marked by a dashed line. Squares PLA-5wt%OMMT batch mixer 100 rpm, circles PLA-3wt%OMMT batch mixer 100 rpm, triangles PLA-3wt% OMMT miniextruder 200 rpm, diamonds PLA-3wt% OMMT miniextruder 100 rpm, stars PLA-3wt%OMMT miniextruder 25 rpm. In each series of symbols, solid symbols correspond to long mixing time, open symbols to intermediate time, and half open symbols to short mixing time; solid line pure PLA; $T=170$ °C

modulus $|G^*| = (G'2 + G''2)^{1/2}$ and the gel point will correspond to a plateau at low complex moduli. Figure 2 shows the van Gurp plots for all the studied samples. From Fig. 2, one can clearly see that for the pure PLA matrix, the curve approaches 90° at low complex moduli, indicating the flow behavior of a viscous fluid. For all processed nanocomposites, the elastic solid-like behavior is observed, i.e., percolating networks of the dispersed nanoclay particles are formed. However, the level of elasticity is very different, indicating different micro/nanostructures of the percolating networks due to different degrees of clay dispersion. The networks in the samples processed in the microextruder consist mostly of microparticles, while the networks in the samples processed in the internal batch mixer include more tactoids and individual silicate sheets (see further TEM results). These dispersed interacting silicate sheets impart higher elasticity to the network. The elasticity and the level of clay dispersion increases with the screw speed (shear rate), mixing time, and polymer concentration and is especially high for the samples compounded in the Haake batch mixer compared to the Minilab microextruder.

Figure 3a and b represents the elastic response (G' at low single frequency $\omega=0.063$ rad/s) as a function of the mixing energy for the nanocomposites processed in the microextruder (Fig. 3a) and in the batch mixer (Fig. 3b). Both plots show progressive increase in the melt elasticity with the mixing energy, i.e., a “master curve” is constructed for each mixer, which reaches saturation of elasticity for the batch mixer (Fig. 3b). However, the melt elasticity level reached in the batch mixer for 3 wt% clay is one order of magnitude higher (200 Pa, Fig. 3b) than the one in the

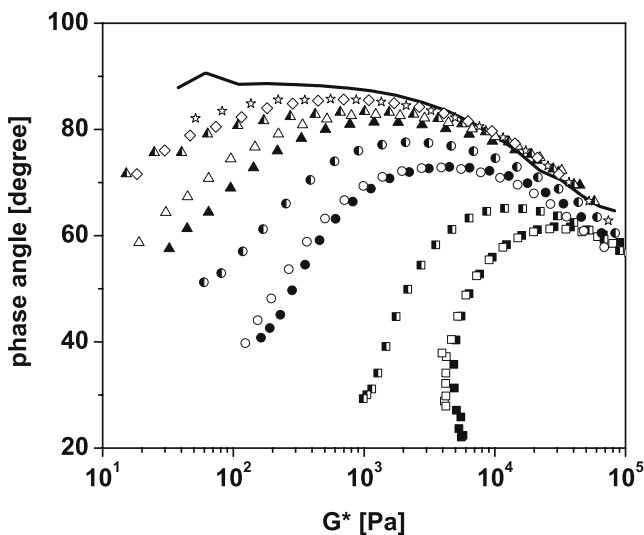


Fig. 2 Phase angle as a function of complex modulus for the PLA, PLA/OMMT-3 wt%, and PLA/OMMT-5 wt% compounded at different processing conditions and in both mixers. Symbols are the same as those specified in Fig. 1

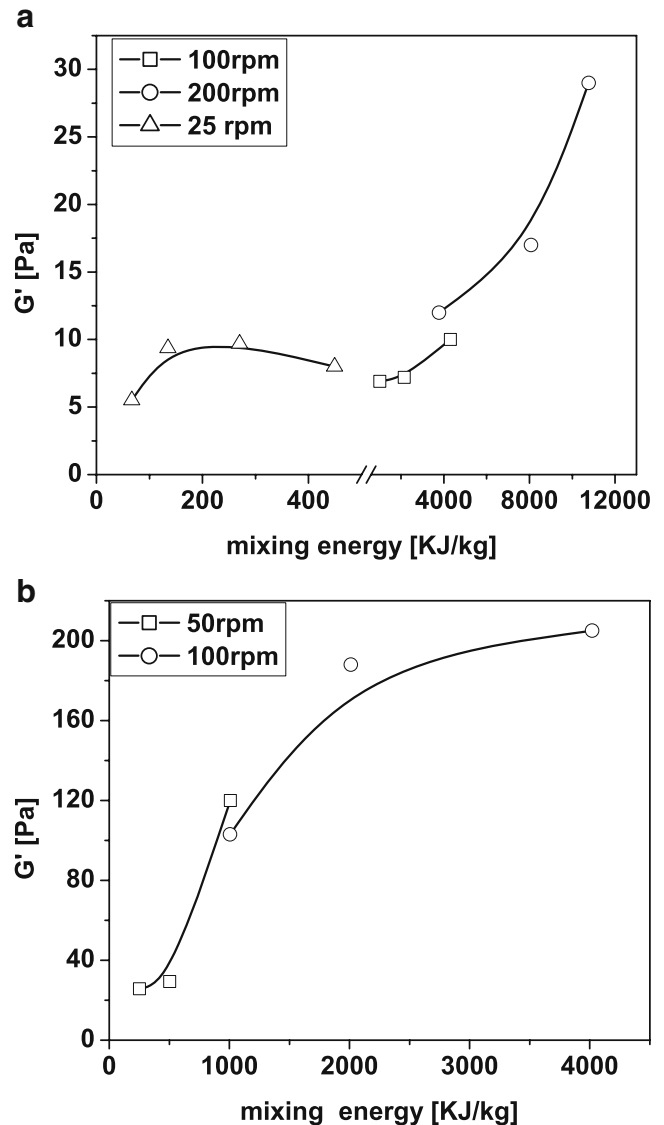


Fig. 3 Elastic modulus at $\omega=0.063$ rad/s as a function of the mixing energy for PLA/OMMT-3 wt% nanocomposites compounded in the microextruder (a) and in the internal batch mixer (b) at various processing conditions

microextruder (30 Pa, Fig. 3a), even though the highest mixing energy in the batch mixer is three times lower. The step increase in elasticity is even more pronounced for the 5 wt% clay where the melt elasticity in the low-frequency region reaches 5,000 Pa (see Fig. 1a).

To explain the differences in the melt elasticity for the samples processed in different mixers, we compare in Fig. 4 the frequency dependence of the complex viscosities. For the samples processed in the batch mixer, the complex viscosity shows a strong rise—deviation from the limiting linear viscoelastic behavior in the terminal zone at $\omega < \omega_c = 1$ rad/s. This rise in η^* is typical for the three-dimensional network formation. Nonlinear rise in η^* is more pronounced for higher clay concentration (5 wt%), see Fig. 4.

The complex viscosities of nanocomposites, processed in the microextruder, in the whole probed frequency range are lower than the viscosity of a pure (nonprocessed) PLA (see Fig. 4) that indicates thermal degradation in the Minilab. The drop in viscosity is stronger for the samples processed at higher screw speeds. Thus, the leading factor of the degradation during PLA–clay processing is a high shear rate developed in the microextruder.

Degradation is an important obstacle in industrial compounding, especially for biodegradable polymers. Degradation decreases the stress developed during processing, which in turn results in poor clay dispersion. Inhomogeneous and low dispersion leads to the loss of valuable mechanical properties in the final product.

To confirm the idea that the melt elasticity of the nanocomposite, measured as G' or $\tan\delta$ values in the terminal zone, senses the degree of clay dispersion, we include TEM micrographs for the PLA/OMMT-3 wt% samples, processed in the internal batch mixer (Fig. 5a and b) and in the Minilab (Fig. 5c). The clay particles in Fig. 5a are in the process of exfoliation: one can clearly see fine morphology. In Fig. 5b at higher magnification, one can possibly see individual platelets. The clay agglomerates in Fig. 5c are in the preliminary stage of intercalation, particles are large and compact. This difference in morphology directly confirms that in the internal batch mixer, a much higher degree of dispersion of clay agglomerates is achieved, although the total mixing energy in the Minilab was two times higher than in the internal batch mixer.

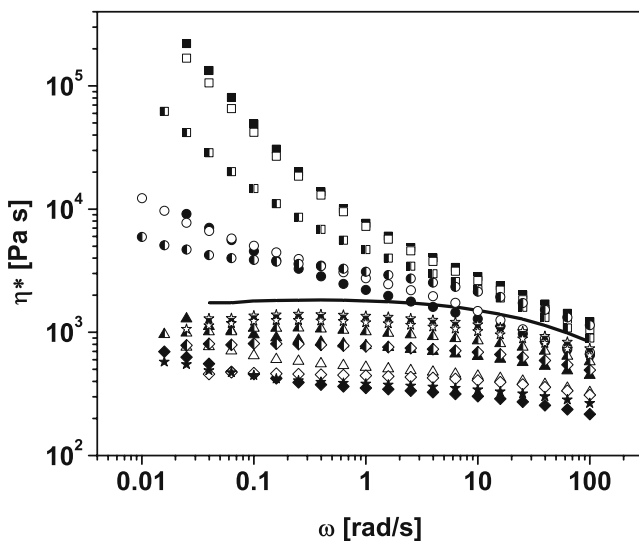


Fig. 4 Evolution of complex viscosity for the PLA, PLA/OMMT-3 wt%, and PLA/OMMT-5 wt% compounded in different mixers and variable processing parameters. *Solid line* pure PLA. Symbols are the same as those specified in Fig. 1

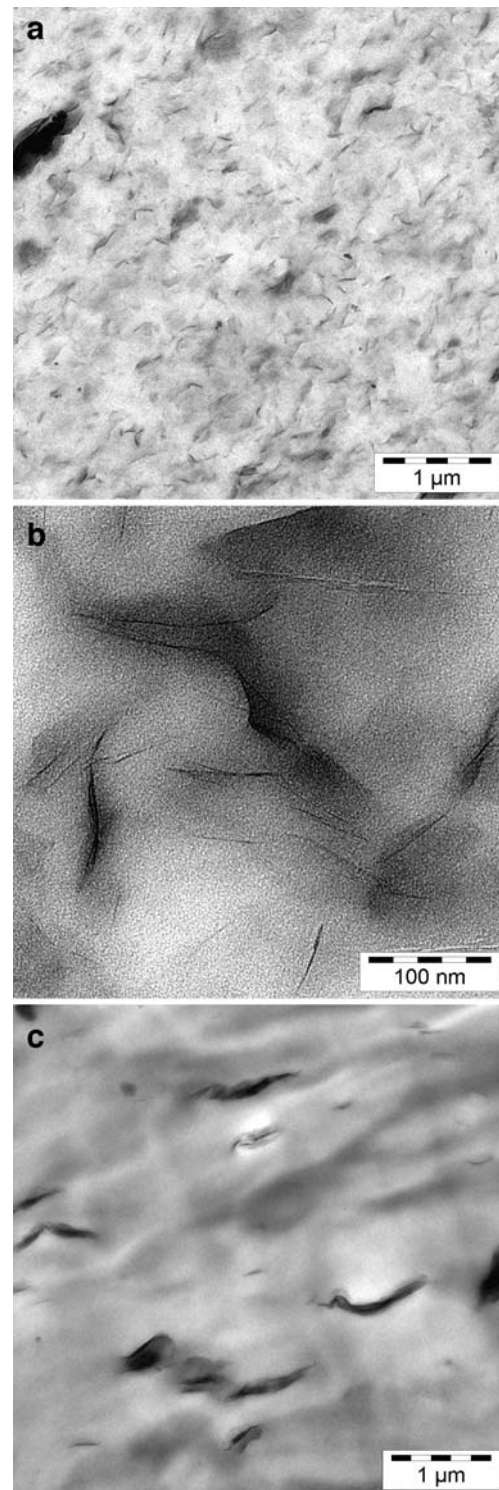


Fig. 5 TEM micrographs taken from PLA/OMMT-3 wt% nanocomposites compounded in both mixers. **a** and **b** were obtained after mixing in the internal batch mixer for 20 min at 100 rpm (mixing energy $E=4,020$ kJ/kg); **c** was obtained after mixing in the Minilab for 15 min at 200 rpm (mixing energy $E=8,073$ kJ/kg). TEM micrographs were taken on Electron Microscope Zeiss LEO 912 Omega

X-ray diffraction

The OMMT diffraction pattern displays one diffraction peak at $2\theta=4.8$, corresponding to d_{001} . The interlayer spacing is calculated from the d_{001} peak using Bragg’s law:

$$d_{00n} = n\lambda / (2 \sin \theta) \tag{5}$$

where n is an integer, θ is the angle of incidence of the X-ray beam, and $\lambda=0.15405$ nm is the X-ray wavelength.

In Fig. 6, the interlayer spacing, d_{001} , for the pure OMMT and for the processed nanocomposites is plotted as a function of the mixing energy. The average value of the interlayer spacing for the nanocomposites is $d_{001}=3.8\pm 0.2$ nm compared to $d_{001}=1.7$ nm for pure OMMT that indicates an intercalated stage. Within the experimental error of these measurements, the interlayer spacing is found to be independent of the type of mixer (batch mixer vs microextruder), processing conditions (screw speed, mixing time), and even clay content (3 and 5 wt%).

While rheological properties show dramatic evolution with mixing energy, the intergallery spacing stays constant. This apparent contradiction comes from the fact that different methods provide different structural characterization. Rheology senses changes in the dispersion state of agglomerates, whereas X-ray diffraction senses local structure, i.e., intercalated stage of clay stacks. The fact that d -spacing is constant shows that we monitor an “average” value of intergallery spacing for the stacks in the intercalated stage, which does not reflect the whole complexity of the structure. It is possible that some other

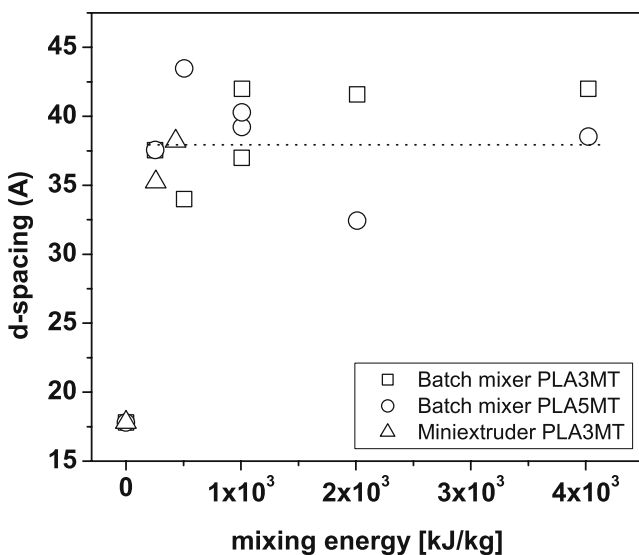


Fig. 6 Interlayer spacing d_{001} of the first peak as a function of mixing energy E for the three PLA/OMMT-3 wt% (squares and triangles) and PLA/OMMT-5 wt% (circles) compounded at different processing parameters in both mixers. The value $d_{001}=17$ A at $E=0$ corresponds to pure OMMT. Dashed line shows the average value from all nanocomposites

morphological units are present, like microparticles or stacks with higher d -spacing, which could not be detected by XRD due to experimental limitations. Thus, XRD, as a method of morphological characterization of clay dispersion, gives information of a limited value and should not be solely used to draw general conclusions about the structure of the nanocomposite.

Other methods need to be explored. A further attempt is made to detect the change of dispersion using light attenuation technique.

Optical studies—light attenuation

The attenuation of the light intensity, after the beam passes through a plate-like sample with thickness D is given by the Lambert–Beer law (Kerker 1969):

$$\frac{I}{I_0} = \exp(-kD) \tag{6}$$

where I_0 is the flux of the light beam at the sample front, I is the flux remaining after the beam has passed through the sample, and k is the linear attenuation coefficient, which is due to both scattering and absorption of light.

As a first approximation, we assume that for the clay agglomerates under study, the turbidity is caused mainly by the scattering and the contribution arising from absorption is negligible for the applied wavelength of $\lambda=633$ nm. At the initial stages, we have clay agglomerates in the length scale of microns. Those microparticles can be considered as spherical in a rough approximation. The amount and size of these microparticles dominate the light attenuation signal. Changes of the attenuation coefficient during the mixing process are due to a progressive decrease of size of clay stacks, which break from microparticles to an intercalated stage and further on possibly to an exfoliated stage.

The theoretical approach applied here is based on the scattering of one spherical particle and is generally applied to a dilute suspension-type system. The distance between particles is assumed to be greater than the diameter of the particle itself. This is true for the initial stage of dispersion process at low clay concentration.

The attenuation coefficient from an assembly of monodisperse isolated spherical particles is given by (Kerker 1969):

$$k = \rho(R)\sigma^2(R) \tag{7}$$

$$\sigma^2(R) = \pi R^2 Q(R) \tag{8}$$

where $\rho(R) = N/V_{total} = 3\varphi/4\pi R^3$ is the number density of scattering particles, N is the total number of scattering particles, V_{total} is the total volume of the cubic lattice, R is the particle’s radius, $\sigma^2(R)$ is the total scattering cross-section, and $Q(R)$ is the “scattering efficiency”, which is a

complex function of particle’s size, and is dependent upon the model. The exact expression for $Q(R)$ is derived only for spherical particles.

The initial stage of the dispersion of microcomposites includes the clay stacks with sizes in the micrometer range. According to theoretical calculations (Kerker 1969; Heck et al. 2006; Fritsch et al. 2006), for the micrometer–nanometer range of scattering particles R is approximately 10^{-6} – 10^{-8} m (which corresponds to the Rayleigh–Debye–Gans [RDG] regime), the scattering efficiency is given by:

$$Q_{RDG} = (m - 1)^2 \left[\frac{5}{2} + 2\alpha^2 - \frac{\sin(4\alpha)}{4\alpha} - \frac{7}{16\alpha^2} (1 - \cos(4\alpha)) \right. \\ \left. + \left(\frac{1}{2\alpha^2} - 2 \right) (0.577 + \ln(4\alpha) + Ci(4\alpha)) \right]$$

$$m = \frac{n_s}{n_m}$$

$$\alpha = \frac{2\pi n_m R}{\lambda}$$

$$Ci(x) = - \int_x^\infty \frac{\cos x'}{x'} dx'$$

(9)

where n_s and n_m are the refractive indices of the scatterer and the surrounding media, respectively. Thus, Eq. 9 links the scattering efficiency of light to the particle’s average size.

The analysis of Eq. 9 shows that for $\alpha > 1$ (which corresponds to the RDG regime), the scattering efficiency scales as the second power of the particle’s radius $Q(R) \sim R^2$. Consequently, the total scattering cross-section scales (according to Eq. 8) as the fourth power of the particle’s radius $\sigma^2 \sim R^4$ and attenuation coefficient (according to Eq. 7) scales linearly with particle’s radius:

$$k \sim \frac{\varphi R^4}{R^3} \sim R \tag{10}$$

Figure 7 represents the attenuation coefficient as a function of mixing energy for different samples processed

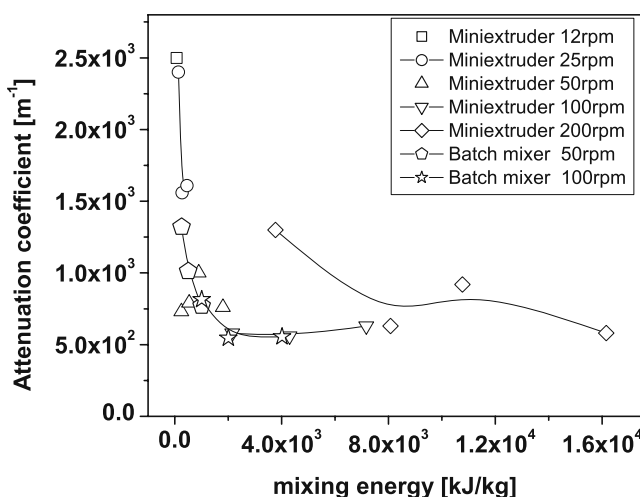


Fig. 7 Light attenuation coefficient k as a function of mixing energy E for PLA/OMMT-3 wt% compounded in both mixers at different processing parameters (screw speed, rpm) as specified on the graph

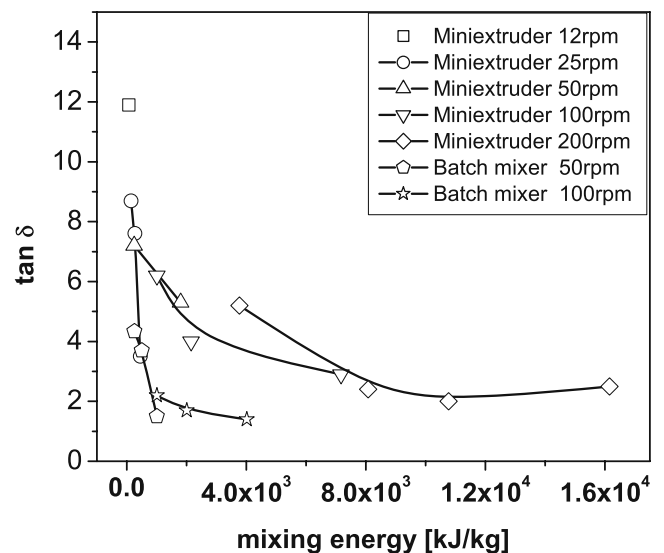


Fig. 8 Loss tangent at $\omega=0.063$ rad/s as a function of mixing energy E for PLA/OMMT-3 wt% compounded in both mixers at different processing parameters (screw speed, rpm) as specified on the graph

in both mixers. The attenuation decreases with the progress of mixing and reaches saturation at high mixing energies. In the frame of the above simplified model, we may expect that the average size of the microparticles also decreases during progressive mixing until it reaches some constant value (Eq. 10).

As it was already stated above, this approach is simplified and does not take into account many factors, which may contribute to light attenuation. Photons, which are scattered by clay particles in forward direction, cannot be separated from the primary beam and contribute to the transmitted intensity and consequently to light attenuation. During the dispersion process, the surface area increases and the system becomes equivalent to the concentrated suspension. In such a case, forward multiple scattering may contribute to light attenuation. Moreover, the absorption of light by nontransparent clay particles may be not negligible and also contribute to light attenuation. The scattering clay particles are polydisperse in size and shape. All this shows that the model for the light attenuation of monodisperse spheres is too simplified for the complex structural architectures of clay agglomerates. However, this attempt may initiate the development of more adequate approaches, which take into account the factors mentioned above.

To compare optical and rheological results, we plot in Fig. 8 the loss tangent ($\tan\delta$) at a single low-frequency $\omega=0.063$ rad/s vs mixing energy for the same samples. $\tan\delta$ decreases with the mixing energy and reaches saturation faster for the samples processed in the batch mixer. One can see a good correlation of the attenuation coefficient in the solid state and loss tangent in melt rheology: with the progress of dispersion, attenuation decreases by a factor of 5 and low-frequency loss tangent by a factor of 6.

The direct correlation between light attenuation coefficient and loss tangent is shown in Fig. 9. Solid and open points represent the samples processed in the internal batch mixer and in the miniextruder, respectively. The experimental dependence $k=f(\tan\delta)$ (points) is approximated by a linear function (solid line) with correlation coefficient $R^1=0.88$ for all the points. One can clearly see from Fig. 9 that linear correlation holds better for the samples processed in the batch mixer (linear fit for the solid points gives correlation coefficient $R^2=0.94$). However, we do not expect the same correlation for the samples processed in the batch mixer and in the miniextruder because these mixers have different geometries and types of the flow.

In summary, the combination of low-frequency loss tangent and light attenuation coefficient provides a potentially sensitive method for the characterization of the degree of clay dispersion. The correlation in rheological and optical responses can open an approach for the rapid inline analysis of the degree of dispersion during melt processing of nanocomposites. One has to keep in mind that $\tan\delta$ is still a function of frequency at low frequencies. In our studies, for the dependence $k=f(\tan\delta)$, we used $\tan\delta$ values at $\omega=0.063$ rad/s. The actual value of chosen frequency does not matter. The only requirement is that it should be in the terminal zone and one and the same for all the compared samples. Studies of different polymer nanocomposite systems are underway to determine how general linear correlation is.

Effect of degree of dispersion on mechanical properties

According to the results presented above, we conclude that nanocomposites processed in the internal batch mixer show

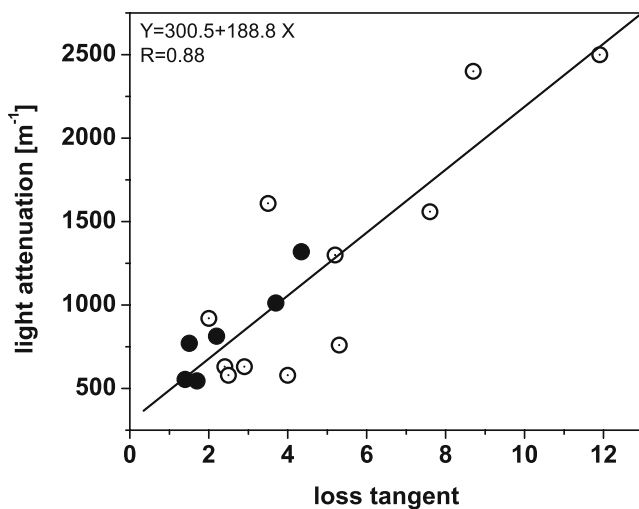


Fig. 9 Light attenuation coefficient vs loss tangent for PLA/OMMT-3 wt% compounded in both mixers: *solid symbols* internal batch mixer, *open symbols* miniextruder. *Straight line* shows the linear fit with correlation coefficient $R=0.88$

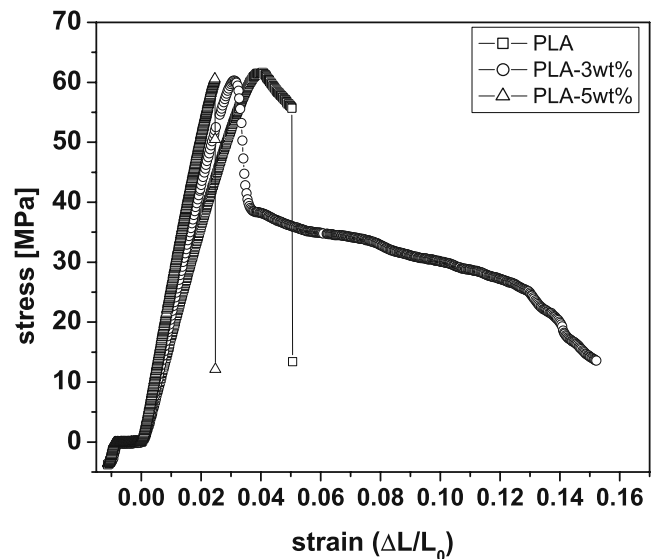


Fig. 10 Stress–strain curves for the PLA, PLA/OMMT-3 wt%, and PLA/OMMT-5 wt% processed at 50 rpm for 20 min in the batch mixer

a reasonable level of clay dispersion. The melt elasticity (elastic modulus G'), loss tangent in the melt, and light attenuation coefficient reach saturation at high mixing energies, which may indicate that a constant level of dispersion is reached. It is essential to check the mechanical properties of these samples because of two reasons. First, to find out whether the degree of dispersion achieved in the processing step imparts the enhanced mechanical properties compared to pure PLA. Second, to understand to what degree the laboratory scale experiments on rheology and optics can be used as control methods of dispersion.

Tensile tests have been carried out on pure PLA samples and all nanobiocomposite samples processed during 5 and 20 min in the Haake internal batch mixer. Figure 10 shows the typical stress–strain curves for pure PLA and PLA/

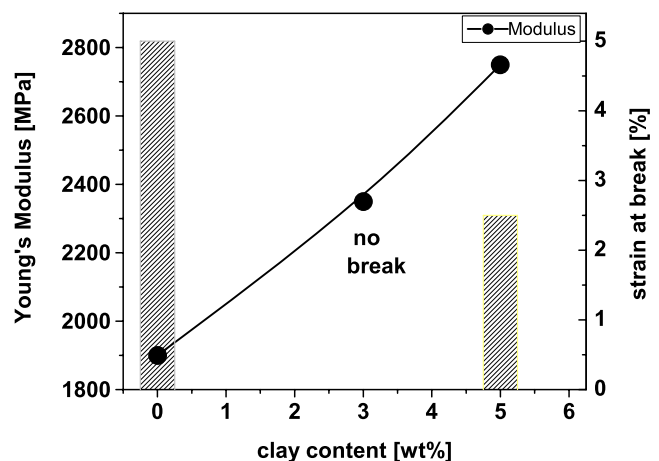


Fig. 11 Young's modulus (circles) and strain at break (bars) for the PLA, PLA/OMMT-3 wt%, and PLA/OMMT-5 wt%

OMMT-3 wt% and PLA/OMMT-5 wt%. The presented results are average values obtained on five samples.

Results on the mechanical properties are summarized in Fig. 11. There are several important points. First, the stiffness of the nanocomposite rises with increasing filler content: Young's modulus increases by 24% for 3 wt% filler and by 45% for 5 wt% filler (Fig. 11). Second, the material becomes more brittle at 5 wt% clay loading because the strain at break decreases twice from 5% for pure PLA to 2.6% for PLA/OMMT-5 wt%. This is a typical situation in processed nanocomposites when the increase in rigidity is accompanied by the increase in brittleness. However, in our case, the addition of 3 wt% C30B increases both the rigidity and ductility because the material does not break (Fig. 11). This important result indicates a good level of dispersion, which leads to a good stress transfer and reasonable optimization of the overall mechanical properties of PLA/OMMT-3 wt%. This interesting finding needs to be confirmed and explored further.

Conclusion

Nanobiocomposites PLA/OMMT have been compounded in the Minilab microextruder and in the internal batch mixer with varying processing conditions. To check the degree of dispersion in processed nanocomposites, the rheological properties have been investigated systematically. Processed PLA/OMMT samples showed percolation in the melt, detected as a step increase in low-frequency elastic moduli compared to pure PLA. The melt elasticity of the nanocomposites increases progressively with mixing energy, which we associate with a progress of dispersion of clay agglomerates and confirm it directly by TEM results.

An attempt was made to characterize the progress of dispersion by melt rheology coupled with light attenuation. The light attenuation coefficient decreases by a factor of 5, low-frequency loss tangent decreases by a factor of 6 with the progress of dispersion, and both characteristics reach saturation, which may be attributed to the maximum level of dispersion achieved in the present experimental conditions. The combination of low-frequency loss tangent and light attenuation coefficient provides a potentially sensitive method for the characterization of the degree of clay dispersion. The direct correlation between light attenuation coefficient and loss tangent follows linear dependence and may open an approach for the rapid inline analysis of the degree of dispersion in melt-processed nanocomposites. Our further studies will explore how general linear correlation is.

TEM results showed directly that the internal batch mixer gave a much better level of dispersion of the nanoclay in the PLA matrix compared to the Minilab

miniextruder. This good level of dispersion translates to the rheological, optical, and further on to the enhanced mechanical properties of PLA nanocomposites. The main reason for the poor dispersion level in the miniextruder and consequent loss in the mechanical properties is the thermal impact of the Minilab on the biodegradable PLA.

The results presented in this study do not allow resolving the whole complexity of the nanocomposite structures; neither do they answer many fundamental questions of the phenomena behind polymer nanocomposites. However, an attempt is made to correlate rheological measurements related to the degree of dispersion with optical characterization, allowing inline process control. Inline characterization with optical probes is underway and will allow direct correlation between dispersion and thermomechanical history, and eventually better fundamental understanding of the dispersing process of clay agglomerates within a polymer matrix. The still open question of the relative importance of shear rate, shear stress, and mixing time in the dispersion process could be addressed in a more quantitative way.

Acknowledgement The authors are grateful for the financial support from the National Agency for Research grant (ANR-05-BLAN-0256-01-France).

References

- Bousmina M (2006) Study of intercalation and exfoliation process in polymer nanocomposites. *Macromolecules* 39:4259–4264
- Bousmina M, Ait-Kadi A, Faisant JB (1999) Determination of shear rate and viscosity from batch mixer data. *J Rheol* 43(2):415–433
- Dennis HR, Hunter DL, Chang D, Kim S, White JL, Cho JW, Paul D (2001) Effect of melt processing conditions on the extent of exfoliation in organoclay-based nanocomposites. *Polymer* 42:9513–9522
- Fornes TD, Yoon PJ, Keskkula H, Paul DR (2001) Nylon 6 nanocomposites: the effect of matrix molecular weight. *Polymer* 42:9929–9940
- Fritsch J, Stille W, Strobl G (2006) Investigation of polymer crystallization kinetics with time dependent light attenuation measurements. *Colloid Polym Sci* 284:620–626
- Heck B, Kawai T, Strobl G (2006) Time dependent light attenuation measurements used in studies of the kinetics of polymer crystallization. *Polymer* 47:5538–5543
- Kadar F, Szazdi L, Fekete E, Pukanszky B (2006) Surface characterization of layered silicates: influence on the property of clay/polymer nanocomposites. *Langmuir* 22:7848–7854
- Kerker M (1969) *The scattering of light*. Academic Press, New York
- Maric C, Macosko CW (2001) Improving polymer blend dispersion in mini-mixers. *Polym Eng Sci* 41:118–130
- Martin O, Avérous L (2001) Poly(lactic acid): plasticization and properties of biodegradable multiphase systems. *Polymer* 42:6209–6219
- Meincke O, Kaempfer D, Weickmann H, Friedrich CH, Vathauer M, Warth H (2004) Mechanical properties and electrical conductivity of carbon-nanotube filled polyamide-6 and its blends with acrylonitrile/butadiene/styrene. *Polymer* 45:739–748

- Pinnovaia TJ, Beall GW (eds) (2001) Polymer–clay nanocomposites. Wiley, New York
- Ray SS, Okamoto M (2003) Polymer/layered silicate nanocomposites: a review from preparation to processing. *Prog Polym Sci* 28:1539–1641
- Szazdi L, Abranyi A, Pukanszky Jr B, Vancso JG, Pukanszky B (2006) Morphology characterization of PP/clay nanocomposites across the length scales of structural architecture. *Macromol Mater Eng* 291:858–868
- Tanoue S, Utracki LA, Garcia-Rajon A, Tatibouet J, Cole KC, Kamal MR (2004) Melt compounding of different grades of polystyrene with organoclay. *Polym Eng Sci* 44:1046–1060
- Utracki LA (2004) Clay-containing polymeric nanocomposites, vols 1 and 2. RAPRA Technology, Shawbury, England
- Wagener R, Reisinger TJ (2003) A rheological method to compare the degree of exfoliation of nanocomposites. *Polymer* 44:7513–7518
- Winter HH, Mours M (1997) Rheology of polymers near liquid–solid transition. *Adv Polym Sci* 134:165–248